2-17-2015

Spin alignment of excited projectiles due to target spin-flip interactions

R. J. Charity
Washington University in St. Louis

J. M. Elson
Washington University in St. Louis

J. Manfredi
Washington University in St. Louis

R. Shane
Washington University in St. Louis

L. G. Sobotka
Washington University in St. Louis

See next page for additional authors

Recommended Citation

Charity, R., Elson, J., Manfredi, J., Shane, R., Sobotka, L., Chajecki, Z., Coupland, D., Iwasaki, H., Kilburn, M., Lee, J., Lynch, W., Sanetullaev, A., Tsang, M., Winkelbauer, J., Youngs, M., Marley, S., Shetty, D., & Wuosmaa, A. (2015). Spin alignment of excited projectiles due to target spin-flip interactions. *Physical Review C - Nuclear Physics, 91* (2) https://doi.org/10.1103/PhysRevC.91.024610

Spin alignment of excited projectiles due to target spin-flip interactions

R. J. Charity, J. M. Elson, J. Manfredi, R. Shane, L. G. Sobotka, Z. Chajecki, D. Coupland, H. Iwasaki, M. Kilburn, Jenny Lee, W. G. Lynch, A. Sanetullaev, M. B. Tsang, J. Winkelbauer, M. Youngs, S. T. Marley, D. V. Shetty, and A. H. Wuosmaa

Phys. Rev. C **91**, 024610 — Published 17 February 2015

DOI: 10.1103/PhysRevC.91.024610

Spin alignment of excited projectiles due to target spin-flip interactions.

R. J. Charity, J. M. Elson, J. Manfredi, R. Shane, and L. G. Sobotka
Departments of Chemistry and Physics, Washington University, St. Louis, Missouri 63130, USA.

Z. Chajecki, D. Coupland, H. Iwasaki, M. Kilburn, Jenny Lee,* W. G. Lynch, A. Sanetullaev, M. B. Tsang, J. Winkelbauer, and M. Youngs
National Superconducting Cyclotron Laboratory and Department of Physics and Astronomy, Michigan State University, East Lansing, MI 48824, USA.

S. T. Marley,† D. V. Shetty, and A. H. Wuosmaa
Department of Physics, Western Michigan University, Kalamazoo, Michigan 49008, USA.

The sequential breakup of E/A=65.5-MeV ^{7}Be and E/A=36.6-MeV ^{6}Li projectiles excited through inelastic interactions with ^{9}Be target nuclei have been studied. For events where the target nucleus remained in its ground state, significant alignment of the excited projectile's spin axis parallel or anti-parallel to the beam direction was observed. This unusual spin alignment was found largely independent of the projectile's scattering angle and it was deduced that the target nucleus has a significant probability of changing its spin orientation during the interaction. It is proposed that the unusual spin alignment is a consequence of the molecular structure of the ^{9}Be nucleus.

PACS numbers: 24.50.+g,25.60.-t,25.70.Ef,24.70.+s,27.20.+n

I. INTRODUCTION

Fragments produced in many nuclear reactions often have a preferred alignment of their spins in some reference frame. Spin alignment is found in a diverse number of reactions including inelastic scattering [1–6], deep elastic scattering [7–10], projectile fragmentation [11–18], fission [19, 20], Coulomb excitation [21] and other direct reactions [22–28]. For peripheral reactions, the dominant angular momentum in the reaction is the initial orbital angular momentum between the projectile and target which is perpendicular to both the beam axis and the reaction plane. It is therefore not surprising that many fragments have their spin aligned, on average, parallel to this direction [7, 11, 12, 21–23, 27]. However there are some cases where different alignments are found [13–16, 18].

Measurement of a fragment's spin alignment can be deduced from its decay products, including β particles though NMR techniques [11, 12], from the recoil induced by gamma-ray decay [23, 24], gamma-ray angular distributions [3, 6, 7, 29], or from the angular distributions of the emitted particles [3, 4, 8, 9, 13, 22, 25–28] or fission fragments [10].

The theory of spin alignment is most tractable in simple direct reactions. Most studies often consider further simplification of the theory, by choosing zero-spin projectile and target nuclei, and zero-spin decay products of the excited projectile. This selection leads to restrictions on the mechanism for producing the spin alignment, i.e., any induced projectile spin must be accompanied by changes in the orbital angular momentum in order to conserve the total angular momentum. However, if the projectile and target nuclei have non-zero spins, then angular momentum conservation can be achieved from changes in the orientation of these spins. Until now, only evidence for small contributions from changes in spin orientation have been found [1].

In this work we examine the spin alignment of ^{6}Li and ^{7}Be projectiles excited via inelastic interactions with a ^{9}Be target. Both projectile and target spins are non-zero; ^{6}Li (J^{π}=1^{+}), ^{7}Be (J^{π}=3/2^{-}) and ^{9}Be (J^{π}=3/2^{-}). We will show that the alignment of the excited projectile's spin axis is quite different from other direct reactions, with a preferred orientation parallel, or anti parallel, to the beam axis. In order to conserve angular momentum, the change in the projectile's spin state is balanced by a flip in the spin orientation of the target nucleus.

Details of the experiment will be discussed in Sec. II and the theory of spin alignment for these direct reactions is given Sec. III. The results of the experiment and their interpretation with the theory are given in Sec. IV. The experimental observations are discussed in terms of target spin flip in Sec. V and finally the conclusions of this work are listed in Sec. VI.

II. EXPERIMENTAL METHOD

The experimental data presented in this work come from a previously published experiment [30, 31] performed at the National Superconducting Cyclotron Laboratory at Michigan State University using the HiRA array [32] to detect projectile-breakup products. Here we

* Now at the University of Hong Kong, Pokflum Road, Hong Kong.
† Now at the Institute for Structure and Nuclear Astrophysics, University of Notre Dame, Notre Dame, In 46656, USA.

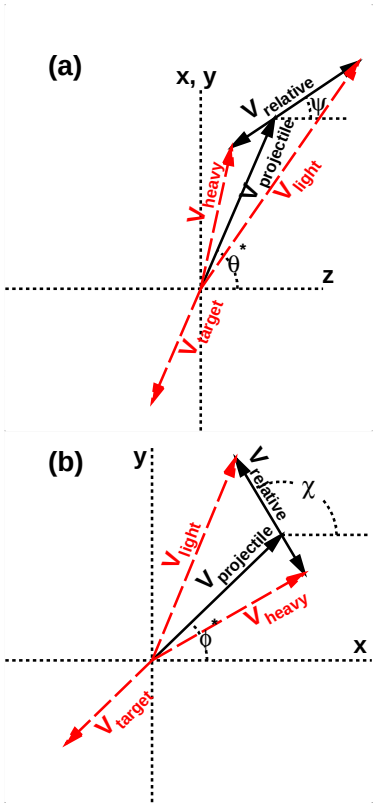

FIG. 1. (Color online) Schematic showing the definition of the angles θ^*, ϕ^*, ψ, and χ in terms of the reaction-center-of-mass velocity vectors of the projectile ($V_{projectile}$) and target (V_{target}) nuclei and those of the light (V_{light}) and heavy (V_{heavy}) decay products of the projectile. The experimental angular correlations were analyzed with the z axis aligned along the beam axis and the x axis in the reaction plane.

present data from the breakup of ^{6}Li and ^{7}Be secondary beams on a 1-mm-thick ^{9}Be target with the same experimental arrangement. Both beams were produced by fragmenting a primary E/A=150-MeV ^{16}O beam with a ^{9}Be target and were separated from other reaction products using the A1900 separator with a momentum acceptance of $\pm$0.5%. The ^{6}Li beam, with an energy E/A=36.6 MeV in the center of the target, was actually a "contaminant" beam of $\sim$35% relative intensity in conjunction with the desired ^{9}C beam. Reactions produced with these two beams were separated using the time of flight measured from the A1900 separator to HiRA. The ^{7}Be beam with E/A=65.2 MeV in the center of the target was $\sim$90% pure. As these secondary beam are produced in fragmentation reactions it is possible they have some small alignment of their spins, but we do not expect this important (see Appendix B).

In these experiments, the HiRA array, consisting of 14 Si-CsI(Tl) $\Delta E - E$ telescopes and located 90 cm downstream from the target, was arranged around all sides of the beam axis to cover the polar angular range from 1.4° to 13°. The double-sided 1.5-mm-thick Si ΔE detectors have 32 strips on both front and back faces thus giving excellent angular resolution for detected fragments. More details of the experimental apparatus and the energy calibrations of the Si and CsI(Tl) detectors can be found in Refs. [30, 31]. In the following section, measured quantities will be presented which have been corrected for the detector bias that has been determined from Monte Carlo simulations (see Appendix A).

III. SEQUENTIAL-DECAY THEORY

Consider a direct binary reaction between a projectile and target with spins (spin projections) of s_p (m_p) and s_t (m_t), respectively. This reaction produces an excited projectile nucleus scattered to an element of solid angle $d\Omega^*$ located at the polar angles θ^* and ϕ^* in the reaction center-of-mass frame. The spin and spin projection of the scattered projectile nucleus are s^* and m^* while those of the scattered target nucleus are s'_t and m'_t. In the center-of-mass frame of the decaying projectile, its lighter decay product is emitted to an element of solid angle $d\Omega$ located at the polar angles ψ and χ. See Fig. 1 for a schematic giving the definition of the various angles. The spins (spin projections) of the lighter and heavier decay products are s_l (m_l) and s_h (m_h), respectively and ℓ is the relative orbital angular momentum of the decay fragments with projection m. To simplify the theory in this study where the heavier decay fragment of the projectile is an α particle, we assume in the following that s_h=m_h=0 and also that the decay of the projectile proceeds through a single value of ℓ.

For clarity and completeness the relevant theory is presented here in the distilled form needed for the present analysis. The angular correlation summed over all spin projections is [33]

$$\frac{d^4\sigma}{d\Omega^* d\Omega} \propto \sum_{m_p,m_t,m'_t,m_l} \left| \sum_{m=-\ell}^{\ell} \alpha_m^{m_p,m_t,m'_t,m_l}(\theta^*,\phi^*) Y_\ell^m(\psi,\chi) \right|^2 . \quad (1)$$

The sum over all m_p and m_t assumes there is no net polarization of the spins of the beam or target nuclei. The spherical harmonics are defined as

$$Y_\ell^m(\psi,\chi) = (-1)^m \sqrt{\frac{2\ell+1}{4\pi}} d^\ell_{m,0}(\psi) e^{im\chi} \quad (2)$$

where Wigner's little-d matrix is

$$d^{\ell}_{m,0}(\psi) = \sqrt{\frac{(\ell-m)!}{(l+m)!}} P^{m}_{\ell}(\cos\psi), \quad d^{\ell}_{-m,0}(\psi) = (-1)^{m} d^{\ell}_{m,0}(\psi), \tag{3}$$

and $P^{m}_{\ell}(\cos\psi)$ are the associated Legendre polynomials.

The coefficients $\alpha_{m}^{m_p,m_t,m'_t,m_l}$ are given by [33]

$$\alpha_{m}^{m_p,m_t,m'_t,m_l}(\theta^*,\phi^*) \propto T^{m+m_l,m'_t}_{m_p,m_t}(\theta^*,\phi^*) \left\langle s_l m_l, \ell m \right| s^* m_l + m \rangle \tag{4}$$

where $T^{m^*,m'_t}_{m_p,m_t}(\theta^*,\phi*)$ is the formation amplitude for the creation of the excited projectile fragment.

For simplicity we replace the projections m_p, m_t, m'_t, m_l, m_h by a single index i in the following. Expanding Eq. (1) we obtain

$$\frac{d^4\sigma}{d\Omega^* d\Omega} \propto \frac{2\ell+1}{4\pi} \sum_{m=-\ell}^{\ell} C_{m,m}(\theta^*,\phi^*) \left| d^{\ell}_{m,0}(\cos\psi) \right|^2 + \sum_{\substack{m_1,m_2 \\ m_1>m_2}} I_{m_1,m_2}(\theta^*,\phi^*,\psi,\chi) \tag{5}$$

where the latter terms are interference terms between the different m projections defined as

$$\begin{aligned} I_{m_1,m_2}(\theta^*,\phi^*,\psi,\chi) &= \sum_i \alpha^i_{m_1}(\theta^*,\phi^*) \left[\alpha^i_{m_2}(\theta^*,\phi^*)\right]^* Y^{m_1}_{\ell}(\psi,\chi) \left[Y^{m_2}_{\ell}(\psi,\chi)\right]^* \\ &+ \sum_i \left[\alpha_{m_1}(\theta^*,\phi^*)\right]^* \alpha^i_{m_2}(\theta^*,\phi^*) \left[Y^{m_1}_{\ell}(\psi,\chi)\right]^* Y^{m_2}_{\ell}(\psi,\chi) \qquad (6) \\ &= 2\frac{2\ell+1}{4\pi}(-1)^{m_1+m_2} d^{\ell}_{m_1,0}(\psi) d^{\ell}_{m_2,0}(\psi) \\ &\times \left\{ \mathrm{Re}\left[C_{m_1,m_2}(\theta^*,\phi^*)\right] \cos(m_1-m_2)\chi - \mathrm{Im}\left[C_{m_1,m_2}(\theta^*,\phi^*)\right] \sin(m_1-m_2)\chi \right\} \qquad (7) \end{aligned}$$

where

$$C_{m_1,m_2}(\theta^*,\phi^*) = \sum_i \alpha^i_{m_1}(\theta^*,\phi^*) \left[\alpha^i_{m_2}(\theta^*,\phi^*)\right]^* \tag{8}$$

and the following symmetry relations are valid

$$I_{m_2,m_1}(\theta^*,\phi^*,\psi,\chi) = I_{m_1,m_2}(\theta^*,\phi^*,\psi,\chi), \quad C_{m_2,m_1}(\theta^*,\phi^*) = C_{m_1,m_2}(\theta^*,\phi^*)^*. \tag{9}$$

The density matrix for the decay orbital angular momentum is a normalized version of the C_{m_1,m_2} matrix [34], i.e.,

$$\rho^{\ell}_{m_1,m_2}(\theta^*,\phi^*) = \frac{C_{m_1,m_2}(\theta^*,\phi^*)}{\mathrm{tr}\left[C_{m_1,m_2}(\theta^*,\phi^*)\right]} \tag{10}$$

where the real diagonal elements give the m-substate probability distribution and the complex non-diagonal elements determine the magnitude and phase of the interference between the different m substates.

As we are free to choose any quantization axis, is it useful to make a choice that simplifies the problem. One such choice is to define the z axis as the beam axis and the x axis is taken to be in the reaction plane, i.e., $\phi^* = 0$. With this choice we find from symmetry considerations [35],

$$T^{-m*,-m'_t}_{-m_p,-m_t}(\theta^*) = (-1)^{m'_t-m_t+m*-m_p} T^{m*,m'_t}_{m_p,m_t}(\theta^*), \tag{11}$$

$$\alpha^{-m_p,-m_t,-m'_t,-m_l,-m_h}_{-m}(\theta^*) = (-1)^{s_l+\ell-s^*}(-1)^{m'_t-m_t-m_l-m_p} \alpha^{m_p,m_t,m'_t,m_l,m_h}_{m}(\theta^*). \tag{12}$$

From these we obtain

$$C_{-m_1,-m_2}(\theta^*) = (-1)^{m_1+m_2} C_{m_1,m_2}(\theta^*), \tag{13}$$

For $m_2 \neq -m_1$, the interference terms can be combined to cancel the $\sin(m_1-m_2)\chi$ terms of Eq. (7), i.e.,

$$I_{m_1,m_2}(\theta^*,\psi,\chi) + I_{-m_2,-m_1}(\theta^*,\psi,\chi) = 4\frac{2\ell+1}{4\pi}(-1)^{m_1+m_2} d^{\ell}_{m_1,0}(\psi) d^{\ell}_{m_2,0}(\psi) \mathrm{Re}\left[C_{m_1,m_2}(\theta^*)\right] \cos(m_1-m_2)\chi \tag{14}$$

While for $m_1 = m = -m_2 \neq 0$ the $\sin(m_1, m_2)$ term is zero as, to satisfy both Eq. (9) and Eq. (13), we require $\mathrm{Im}\left[C_{m,-m}(\theta^*)\right] = 0$. In general, the angular correlation for $\ell > 0$ is

$$\frac{d^4\sigma}{d\Omega^* d\Omega} \propto \frac{2\ell+1}{4\pi}\left\{C_{0,0}(\theta^*)|d^\ell_{0,0}(\psi)|^2 + 2\sum_{m=1}^{\ell}\left|d^\ell_{m,0}(\psi)\right|^2\left[C_{m,m}(\theta^*) + (-1)^m C_{m,-m}(\theta^*)\cos 2m\chi\right]\right.$$
$$\left. +4\sum_{\substack{1\leq m_1\geq \ell \\ -m_1 > m_2 > m_1}} \mathrm{Re}\left[C_{m_1,m_2}(\theta^*)\right](-1)^{m_1+m_2} d^\ell_{m_1,0}(\psi) d_{m_2,0}(\psi)\cos(m_1 - m_2)\chi\right\} \quad (15)$$

In summary with the chosen quantization axis, the angular correlations are determined by the C_{m_1,m_2} matrix or alternatively the density matrix $\rho^\ell_{m_1,m_2}$. Only real matrix elements enter Eq. 15, or where the matrix elements are complex, only the real components are needed. Information on the imaginary components would require a polarized beam or target.

A. Projections

As $\int_0^{2\pi}\cos m\chi\, d\chi = 0$ for $m \neq 0$, if we project the correlation distribution on the ψ axis, then all the interference terms will drop out and the projected distribution will be given by

$$W(\psi) \propto \frac{2\ell+1}{2}\left[\rho^\ell_{0,0}(\theta^*) + 2\sum_{m=1}^{\ell}\rho^\ell_{m,m}(\theta^*)\left|d^\ell_{m,0}(\psi)\right|^2\right]. \quad (16)$$

As $\int_0^\pi d^\ell_{m_1,0}(\psi) d^\ell_{m_2,0}(\psi)\sin\psi\, d\psi = 0$ for $m_1 - m_2 = $ odd, then by projecting on the χ axis, only the $\cos m\chi$ terms with even m will survive. The projected χ correlations can then be written as

$$W_{even}(\chi) = \int_0^\pi \frac{d^4\sigma}{d\Omega^* d\Omega}\sin\psi\, d\psi \quad (17)$$
$$= A_0 + A_2\cos 2\chi + ... + A_{2\ell}\cos 2\ell\chi. \quad (18)$$

If ℓ is not known, then the highest order term in Eq. (18) needed to fit a measured distribution can give a lower limit to this quantity. To see the odd-m $\cos m\chi$ terms, we construct the quantity

$$W_{odd}(\chi) = \int_0^{\pi/2}\frac{d^4\sigma}{d\Omega^* d\Omega}\sin\psi\, d\psi - \int_{\pi/2}^{\pi}\frac{d^4\sigma}{d\Omega^* d\Omega}\sin\psi\, d\psi \quad (19)$$
$$= A_1\cos\chi + ... + A_{2\ell-1}\cos(2\ell-1)\chi \quad (20)$$

IV. EXPERIMENTAL RESULTS

A. ^{7}Be Breakup

The ^{7}Be nucleus has a strong ^{3}He-α cluster structure and large ^{3}He+α breakup yield. The distribution of target excitation energy E^*_t for all detected ^{3}He + α events, determined from conservation of energy and momentum, is displayed in Fig. 2(a). A strong peak at $E^*_t \sim 0$ MeV is very prominent in this spectrum with a FWHM of around 12 MeV. This width is consistent with the expected resolution as demonstrated by the smooth curve in Fig. 2(a) which is a simulated distribution for E^*_t=0. Thus the experimental peak in this figure predominantly contains events where the target remains in its ground state, however one cannot rule our some contribution from low-lying excited states in ^{9}Be. In the following we will only consider the events in the E^*_t=0 peak as the high-energy tail does not exhibit strong alignment of the projectile.

The ^{7}Be excitation-energy distribution (corrected for the energy-dependent detector efficiency) is shown in Fig. 2(b). This excitation energy, E^*_p, is determine from the invariant mass of the detected ^{3}He-α pair minus the ground-state mass of ^{7}Be and the simulated resolution is 245 keV FWHM at E^*_p=4.6 MeV. This distribution shows a very prominent peak associated with the second excited state (s^*=7/2$^-$) of ^{7}Be at E^*_p=4.57 MeV. The third excitation state (s^*=5/2$^-$) at E^*_p=6.73 MeV is present, but weakly populated.

The angular distribution (corrected for the detector acceptance) for the 7/2$^-$ state is displayed in Fig. 2(c) and shows diffractive oscillations typically expected for inelastic excitations. To accurately define the reaction plane and the breakup angle χ, we restrict further analysis to $\theta^*_{lab} > 2^\circ$, unless specified.

The raw experimental 2-dimensional $\cos\psi - \chi$ angular correlations for the 7/2$^-$ state are shown in Fig. 3(a), while the simulated detection efficiency is displayed in Fig. 3(b). The efficiency-corrected correlation obtained from dividing the raw data by this efficiency is shown in Fig. 3(c). It contains well-defined modulations which can be related to the interference between different m projections.

From angular-momentum and parity conservation, the decay of this ^{7}Be level must be ℓ=3 and the theoretical correlation of Eq. (15) can be defined by 16 unique C_{m_1,m_2} parameters or the equivalent density matrix $\rho^\ell_{m_1,m_2}$ parameters [see Eq. (10)]. These include 7 real matrix elements $\rho^\ell_{0,0}$, $\rho^\ell_{1,1}$, $\rho^\ell_{2,2}$, $\rho^\ell_{3,3}$, $\rho^\ell_{1,-1}$, $\rho^\ell_{2,-2}$, and $\rho^\ell_{3,-3}$ and the real parts of 9 complex matrix elements. Figure 3(d) shows a fit obtained by varying these 16 pa-

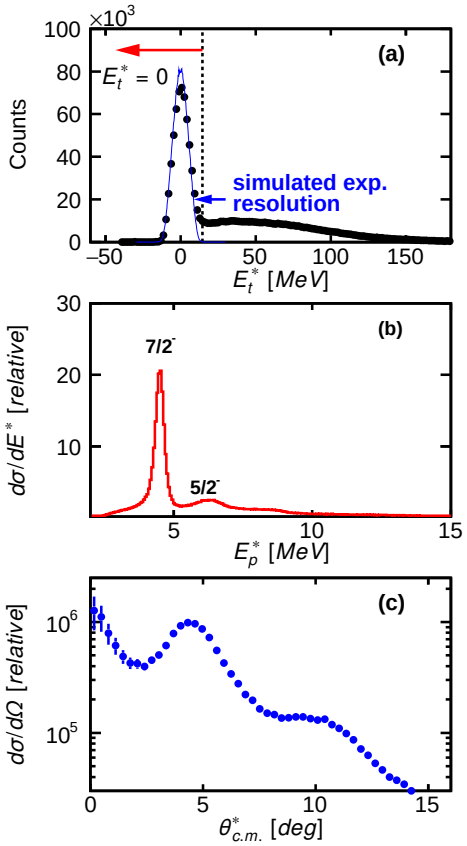

FIG. 2. (Color online) (a) Experimental distribution of the excitation energy of the ^{9}Be target nucleus deduced from detected ^{3}He+α events obtained with the ^{7}Be beam. (b) Distribution of ^{7}Be projectile excitation energy associated with detected events where the target remained in it ground state [E^*_t=0]. (c) Angular distribution of the scattered projectile in the reaction center-of-mass frame for the E^*=4.57-MeV, s^*=7/2$^-$ excited state of ^{7}Be with E^*_t=0.

rameters. This fit reproduces the basic features of the experimental angular correlations quite well.

The fitted density matrix elements are listed in Table I. If we define the reduced matrix elements as

$$c_{m1,m2} = \frac{\rho^l_{m_1,m_2}}{\sqrt{\rho^l_{m_1,m_1}\rho^l_{m_2,m_2}}}, \qquad (21)$$

then, from the Cauchy-Schwarz inequality

$$|\sum_i a_i b_i|^2 \le \sum_i |a_i|^2 + \sum_i |b_i|^2, \qquad (22)$$

it is easy to show that $|\mathrm{Re}\ [c_{m_1,m_2}]| \le 1$. The real components of the reduced matrix elements are also listed in Table I and their magnitudes are indeed less than unity and thus consistent with theory.

To examine the angular correlations in more detail, let us look at the projections discussed in Sec. III A. The experimental correlation projected on the $\cos\psi$ axis, shown in Fig. 4(a), depends only on the real matrix elements

TABLE I. The values of the density matrix $\rho^\ell_{m_1,m_2}$ obtained from fitting to the experimental $\cos\psi$ - χ angular correlation measured for the s^*=7/2 excited state of ^{7}Be. The interference terms are arranged by the order of their $\cos m\chi$ term. Real components of the reduced density matrix Eq. (21) are also shown in the third column.

parameter	fitted value	reduced value
$\rho^\ell_{0,0}$	0.028(1)	1
$\rho^\ell_{1,1}$	0.051(1)	1
$\rho^\ell_{2,2}$	0.122(2)	1
$\rho^\ell_{3,3}$	0.312(2)	1
	$\cos\chi$	
Re $[\rho^\ell_{3,2}]$	-0.052(2)	-0.26(1)
Re $[\rho^\ell_{2,1}]$	-0.024(1)	-0.30(1)
Re $[\rho_{1,0}]$	-0.006(1)	-0.16(3)
	$\cos 2\chi$	
Re $[\rho^\ell_{3,1}]$	-0.027(2)	-0.21(2)
Re $[\rho^\ell_{2,0}]$	-0.026(2)	-0.45(3)
$\rho^\ell_{1,-1}$	-0.031(2)	-0.61(4)
	$\cos 3\chi$	
Re $[\rho^\ell_{3,0}]$	0.011(2)	0.12(2)
Re $[\rho^\ell_{2,-1}]$	0.005(1)	0.07(1)
	$\cos 4\chi$	
Re $[\rho^\ell_{3,-1}]$	0.042(2)	0.33(2)
$\rho^\ell_{2,-2}$	-0.055(2)	0.45(2)
	$\cos 5\chi$	
Re $[\rho^\ell_{3,-2}]$	-0.004(1)	-0.02(1)
	$\cos 6\chi$	
$\rho^\ell_{3,-3}$	0.037(2)	0.12(2)

$\rho^\ell_{m,m}$. Surprisingly, this distribution peaks at ψ=90° ($\cos\psi$=0), i.e., the sequential decay of the ^{7}Be s^*=7/2$^-$ level is dominated by transverse emissions to the beam axis.

The fitted projection is indicated in Fig. 4(a) by the solid curve, together with the contributions from the different $|m|$ values (dashed curves). The fitted $\rho^\ell_{m,m}$ values give the probability distribution of the various m projections, also known as the magnetic-substrate population. Note from Eq. (13), the distribution is symmetric around m=0, i.e., $\rho^\ell_{-m,-m} = \rho^\ell_{m,m}$. This probability distribution is displayed in Fig. 4(b) and is dominated by the $|m|=\ell$ components, i.e., in classical terms, the alignment is mostly parallel or antiparallel to the beam axis a result which is consistent with the strongly transverse decay pattern. This alignment distribution is very unusual in inelatic scattering and this is the most important result of this work.

The $\rho^l_{m_1,m_2}$ density matrix gives information on the alignment of the orbital angular momentum produced in the decay of the excited projectile. However, it would be more interesting to deduce the alignment of the spin of the excited projectile itself. This is described by the

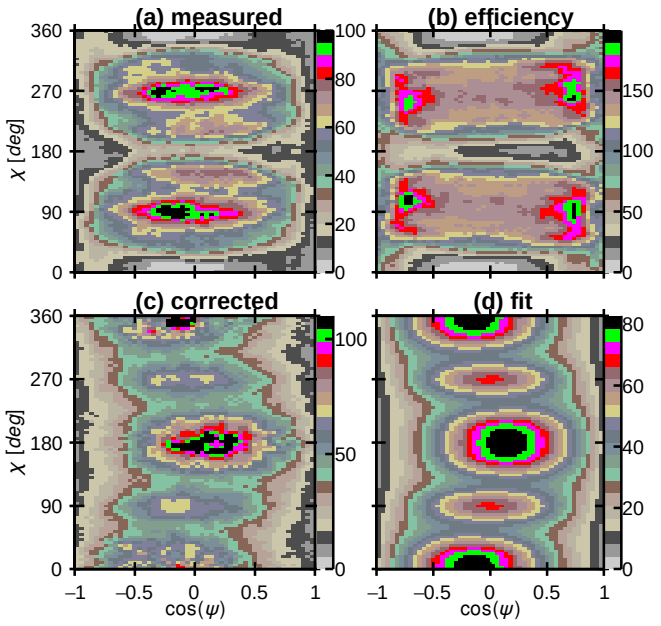

FIG. 3. (Color online) $\cos\psi - \chi$ angular correlation plots obtained for the s^*=7/2$^-$ excited state in ^{7}Be with $\theta^*_{lab} > 2^\circ$. (a) directly measured raw angular correlations without corrections, (b) Simulated detector efficiency, (c) measured correlations corrected for the detected efficiency (d) fitted correlation using Eq. (15).

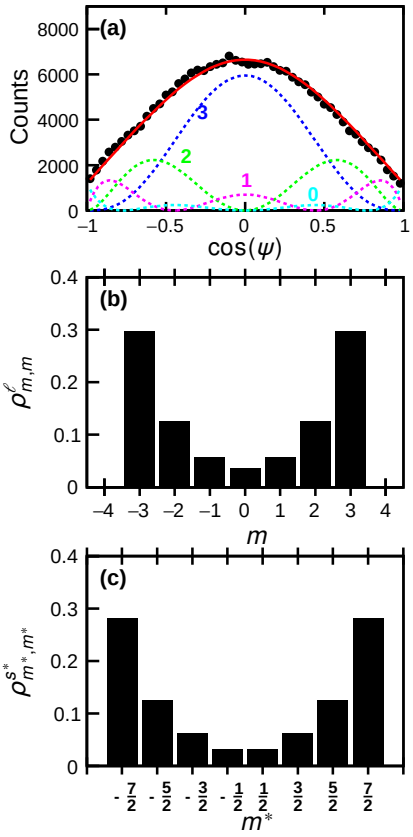

FIG. 4. (Color online) (a) The efficiency-corrected correlation plot for the s^*=7/2$^-$ excited state of ^{7}Be projected on the $\cos\psi$ axis. (b) Probability distribution for the projection m of the decay orbital angular momentum. (c) Probability distribution for the projection m^* of the ^{7}Be spin. In (a), the solid curve shows a fit with the individual m components indicated by the dashed curves.

density matrix [34]

$$\rho^{s^*}_{m_1,m_2}(\theta^*) = \frac{\sum_{m_p,m_t,m_t'} T^{m_1,m_t'}_{m_p,m_t}(\theta^*)\left[T^{m_2,m_t'}_{m_p,m_t}(\theta^*)\right]^*}{\mathrm{tr}\left[\sum_{m_p,m_t,m_t'} T^{m_1,m_t'}_{m_p,m_t}(\theta^*)\left[T^{m_2,m_t'}_{m_p,m_t}(\theta^*)\right]^*\right]}. \quad (23)$$

Although it is not possible to constrain all elements of this matrix from our measured data, the real diagonal elements which give the m-substate distribution can be determined from the diagonal elements of $\rho^\ell_{m,m}$. From Eqs. (4,10,23) we obtain

$$\rho^\ell_{3,3}(\theta^*) = \rho^{s^*}_{\frac{7}{2},\frac{7}{2}}(\theta^*) + \frac{1}{7}\rho^{s^*}_{\frac{5}{2},\frac{5}{2}}(\theta^*), \quad (24)$$

$$\rho^\ell_{2,2}(\theta^*) = \frac{6}{7}\rho^{s^*}_{\frac{5}{2},\frac{5}{2}}(\theta^*) + \frac{2}{7}\rho^{s^*}_{\frac{3}{2},\frac{3}{2}}(\theta^*), \quad (25)$$

$$\rho^\ell_{1,1}(\theta^*) = \frac{5}{7}\rho^{s^*}_{\frac{3}{2},\frac{3}{2}}(\theta^*) + \frac{3}{7}\rho^{s^*}_{\frac{1}{2},\frac{1}{2}}(\theta^*), \quad (26)$$

$$\rho^\ell_{0,0}(\theta^*) = \frac{8}{7}\rho^{s*}_{\frac{1}{2},\frac{1}{2}}(\theta^*) \quad (27)$$

where the coefficients of each term are the square of Clebsch-Gordan coefficients. After solving for $\rho^{s^*}_{m*,m*}$, the m-substate distribution for the s^* spin alignment is plotted in Fig. 4(c). It also shows the alignment is mostly parallel or antiparallel to the beam axis.

An alternative way of specifying the m-substate distribution is via the statistical or polarization tensor ρ_{kq} (or B^q_k in some studies) [34]. The ρ_{k0} terms just depend on the diagonal elements of the density matrix and only even k values are non-zero when $\rho^{s^*}_{m^*,m^*} = \rho^{s^*}_{-m^*,-m^*}$. The ρ_{00} term is just the normalization of the m-substate distribution, and the lowest-order term of interest is ρ_{20}. However, additional terms, ρ_{40} amd ρ_{60}, are necessary to fully describe the distributions in Figs. 4(b) and 4(c) and q >0 terms are needed to describe the off-diagonal elements. An alignment parameter,

$$A = \frac{\rho_{20}}{\rho^{max}_{20}} = \sum_{m^*} \frac{3m^{*2} - s^*(s^*+1)}{s^*(2s^*-1)}\rho^{s^*}_{m^*,m^*}, \quad (28)$$

is often defined where ρ^{max}_{20} is the maximum value of ρ_{20} when only the $|m^*| = s^*$ elements are non-zero. Negative aligment would correspond to a prepondance of the small $|m^*|$ values. The alignments associated with spin of the excited state and it decay orbital angular momentum in this case can be shown to be identical from Eqs. (24-27). We obtain an alignment of A=49(1)% from the experimental data. This is quite large. In comparison typical positive alignments of the order of 10% or less have been found in projecticle fragmentation reactions when the projectile remnants at the peak of their momentum

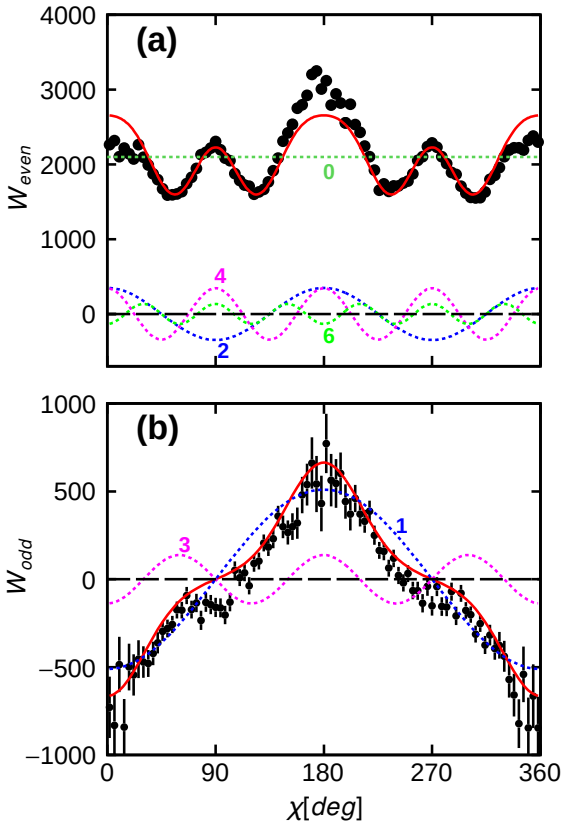

FIG. 5. (Color online) Projected (a) W_{even} and (b) W_{odd} correlation distributions for the s^*=7/2$^-$ excited state of ^{7}Be. The solid curves show fits with Eqs. (18) and (20) while the dashed curves give indivudal the $\cos m\chi$ componets where each curve is labeled by the value of m.

distribution are selected (see appendix B).

By projecting on the χ axis, we highlight the interference terms where m_1-m_2 is even. The angular correlations projected on the χ axis is plotted in Fig. 5(a). By visual inspection, it is clear that $\cos 2\chi$ and $\cos 4\chi$ interference terms are needed to reproduce this distribution. The solid curve shows a fit with Eq. (18) and the four fitted components are indicated by the dashed curves. The fit reproduces the main features of the experimental projection and indicates the presence of some $\cos 6\chi$ component. However the fit would be improved with the addition of some $\cos\chi$ component. The $\cos\chi$ component is quite strong in the 2-dimensional correlation, but it should be zeroed out when projecting on the χ axis (Sec. III A). The presence of some of the $\cos\chi$ component leaking into this plot may be consequence of the deficiencies of the simulated efficiencies. Alternatively it could be associated with the small background under the s^*=7/2$^-$ peak.

The odd-m $\cos m\chi$ terms can be accentuated by the W_{odd} distribution of Eq. (19) which is plotted in Fig. 5(b). In this case, the data points were obtained from the experimental χ distributions gated on ψ <90° and ψ >90°. These two distributions were corrected for their individual detection efficiencies and subtracted. This final distribution clearly has a very strong $\cos\chi$ component and a smaller, but still significant, $\cos 3\chi$ component. A fit with Eq. (20) is indicated by the solid curve and the fitted components are again plotted as the dashed curves. No significant $\cos 5\chi$ component is needed in this fit.

Both the W_{even} and W_{odd} distributions of Fig. 5 clearly show the presence of many interference terms. The density matrix elements in Table I indicate that the detected events are not associated with just a single projection of ℓ, but contain admixtures of different m values. These admixtures are not just between neighboring values of m ($\cos\chi$ terms), and in particular the $\cos 4\chi$ terms in Table I are quite strong. The latter correspond to admixtures for m values separated by 4 units.

B. Scattering-Angle Dependence

The dependence of the angular correlations on the scattering angle θ^* is quite small. To demonstrate this, we have subdivided the events into two approximately equal groups, one with $2° < \theta^*_{lab} < 4.5°$ and the other for larger angles. The two efficiency-corrected angular correlations are plotted in Fig. 6. The result for $\theta^*_{lab} > 4.5°$ has a number of "holes" where the efficiency is zero. However apart from these "holes", the two correlations look very similar with the same dominant features.

For a more quantitative comparison, the m-substate distributions determined from the fitted $\rho^{\ell}_{m,m}$ matrix elements are compared in Fig. 7. In addition to the previously defined θ^* angular range, we also consider events for $\theta^* < 2°$. Even though it is problematic to define a χ angle for such events, the ψ angle is still well defined and the $\rho^{\ell}_{m,m}$ matrix elements can be determined from Eq. (16).

The m-substate distributions for both data sets with $\theta^* > 2°$, which account for most of the events, are similar. The events for $\theta^* < 2°$ again show qualitatively similar behavior with the $|m| = \ell$ components still dominant, but now the m=0 component is somewhat more prominent. Again note that these events account for only a small fraction of the total. Overall there is very little dependence on the scattering angle θ^* and even the changes at very small angles are minor.

C. ^{6}Li breakup

Similar spin alignment is also observed from the d+α breakup of ^{6}Li. Detected d+α events are again found to have a prominent component with E^*_t=0. The projectile excitation-energy distribution for this component is shown in Fig. 8(a). This spectrum shows a dominant peak associated with the E^*_p=2.186-MeV, s^*=3$^+$ first excited state and a smaller peak associated with the E^*_p=4.31-MeV, s^*=2$^+$ third excited state. For the s^*=3$^+$

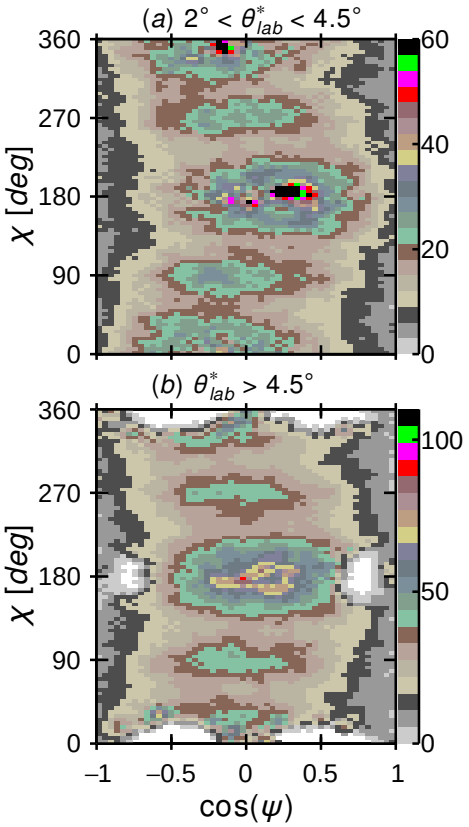

FIG. 6. (Color online) Efficiency-corrected correlation plots for the s^*=7/2$^-$ excited sate of ^{7}Be for the two indicated gates on the projectile scattering angle θ^*.

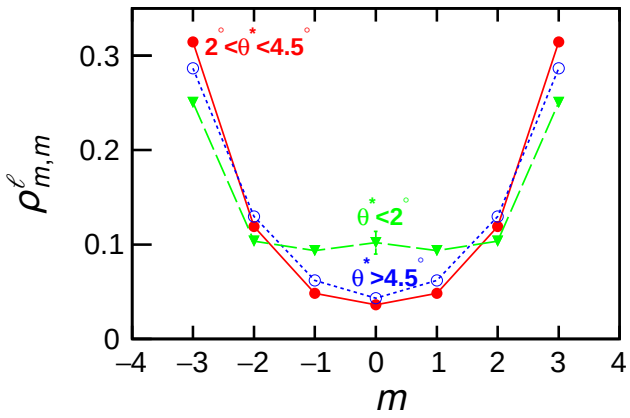

FIG. 7. (Color online) Probability distribution of the projection m of the decay orbital angular momentum for three region of laboratory scattering angle obtained for the s^*=7/2$^-$ excited state of ^{7}Be.

TABLE II. As for Table I, but now for the s^*=3$^+$ excited state of ^{6}Li.

parameter	fitted value	reduced value
$\rho^{\ell}_{0,0}$	0.066(1)	1
$\rho^{\ell}_{1,1}$	0.115(1)	1
$\rho^{\ell}_{2,2}$	0.351(2)	1
	cos χ	
Re $[\rho^{\ell}_{2,1}]$	-0.024(1)	-0.12(1)
Re $[\rho^{\ell}_{1,0}]$	-0.020(1)	-0.23(3)
	cos 2χ	
Re $[\rho^{\ell}_{2,0}]$	-0.050(2)	-0.33(3)
$\rho_{1,-1}$	0.049(2)	-0.43(4)
	cos 3χ	
Re $[\rho^{\ell}_{2,-1}]$	0.005(1)	0.02(1)
	cos 4χ	
$\rho^{\ell}_{2,-2}$	-0.062(2)	0.18(2)

peak, the angular distribution of the scattered projectile is plotted in Fig. 8(b). It has similar features to that found for the ^{7}Be$_{7/2^-}$ level in Fig. 2(c).

For the s^*=3$^+$ state, ℓ=2 and ℓ=4 components are both possible. In the following we will assume only the ℓ=2 decay occurs. The ℓ=4 decay could generate interference terms up to order cos 8χ, but no indication of such higher-order interference terms were observed in the experimental correlations.

The efficiency-corrected angular correlation for the s^*=3$^+$ state, shown in Fig. 9(a), is qualitatively similar to the results for ^{7}Be [Fig. 3(c)]. Again the fitted distribution shown in Fig. 9(b) reproduced the major features of the experimental distribution. The fitted matrix elements are listed in Table II and again the real reduced matrix elements (third columnn) have magnitudes less than unity as expected.

The projected cos ψ distribution for the s^*=3$^+$ state is displayed in Fig. 10(a) and again shows a predominance for traverse decay. The extracted m-substate distribution is plotted in Fig. 10(b) and shows strong alignment with the $|m|$=ℓ components again having the largest probability. Thus they are also consistent with an alignment mostly parallel or antiparallel to the beam axis. The alignment obtain from this distribution is A=51(1)%, very similar to the A=49(1)% value obtained for the s^*=7/2$^-$ state in ^{7}Be.

The $W_{even}(\chi)$ and $W_{odd}(\chi)$ projected distributions for the s^*=3$^+$ state are plotted in Fig. 11 and again are qualitatively similar to the results for ^{7}Be in Fig. 4.

V. DISCUSSION

These sequential breakup reactions are peripheral and are expected to be confined to a narrow window of incoming and outgoing orbital angular momentum, L_{in} and L_{out}, respectively [36]. A number of experimental studies have looked at spin alignment in reactions where the spins of the initial and final products are zero [22, 25–28]. While this greatly simplifies the theory of spin alignment, it also forces a certain type of spin alignment as the spin of the excited projectile can only be obtained from changes in the orbital angular momenta, i.e., by

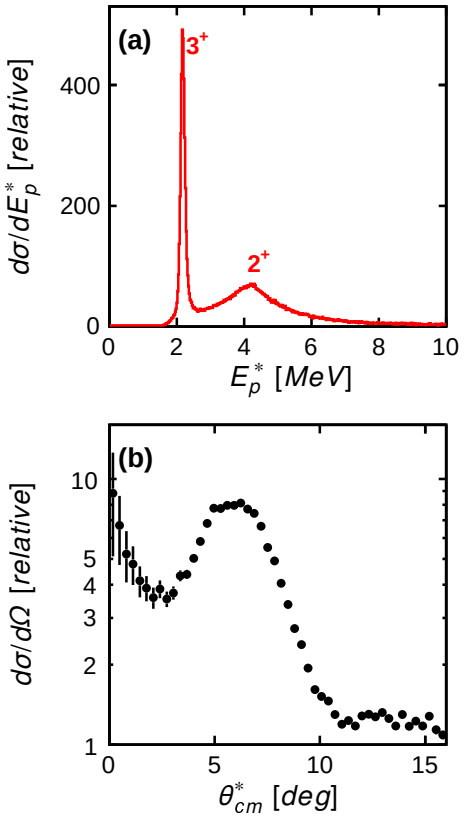

FIG. 8. (Color online) (a) Efficiency-corrected projectile excitation-energy distribution determined from detected d + α events for E_t^*=0 with the ^{6}Li beam. (b) Angular distribution of the scattered projectile extracted for the s^*=3$^+$ level.

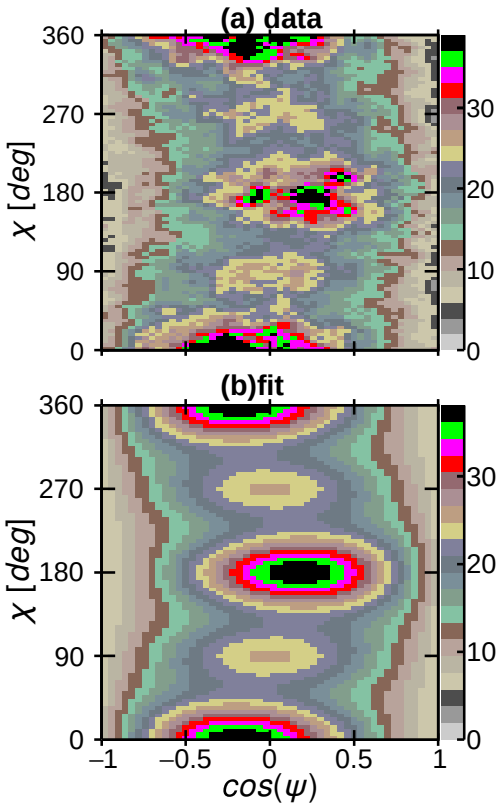

FIG. 9. (Color online) $\cos\psi$-χ angular correlation plots obtained for the s^*=3$^+$ excited state in ^{6}Li with $\theta^*_{lab} > 2°$. (a) efficiency-corrected experimental data. (b) fitted correlation using Eq. (15).

angular-momentum conservation, $s^* = |\boldsymbol{L_{in}} - \boldsymbol{L_{out}}|$ and the observed average spin alignment is typically normal to the reaction plane (parallel to $\boldsymbol{L_{in}}$). If m_{out} is the projection of $\boldsymbol{L_{out}}$ and as different values of m_{out} peak at different scattering angles θ^*, then by gating on θ^*, one is selecting a different m_{out} distribution. If all the spins of the initial and final particles are zero, then m^*=-m_{out}, and the alignment is strongly coupled to the scattering angle [25]. This explains the strong correlations between ψ and θ^* observed in many reactions.

In contrast in this work where, the spins of the initial fragments are nonzero and one of the exit-channel fragments has finite spin, we find only a very weak dependence of the ψ distributions on θ^* and the observed alignment is mostly parallel or anitparallel to the beam axis. These observations suggest that changes in the orbital angular momentum play a significantly smaller role in these reactions. In fact if $\Delta\ell = |\boldsymbol{L_{in}} - \boldsymbol{L_{out}}|$=0, then there is only one projection, i.e. $m_{out} = 0$, and the angular correlations would be independent of scattering angle θ^*.

For $\Delta\ell$=0, the increased spin of the projectile during the reaction could be compensated by changes in the spin projection of the target. For example, if the ^{9}Be target's spin (3/2 $\hbar$) is fully flipped, then this changes the angular momentum by 3 $\hbar$, enabling the excited ^{7}Be projectile's spin to obtain values between $1/2^-$ to $9/2^-$. For the ^{6}Li, this spin flip of the target would enable the excitation of states with spin from 0^+ to 4^+. For both projectiles, these spin ranges allow for the production of the excited states observed in Figs. 2(b) and 8(a).

Addition evidence for significant $\Delta\ell$=0 contribution can be obtained from the θ^* angular distributions in Figs. 2(c) and 8(b). Only for $\Delta\ell$=0, do the angular distributions have a peak at θ^*=0 [36] as observed in these experimental distribution. Thus we have presented a number of pieces of evidence that point to changes in the target's spin orientation, rather than changes in the orbital angular momentum, as the most important source of the increased spin of the excited projectile. Although spin flip in inelastic scattering has been observed before, it only contributed to a small fraction of the total yield (∼1%) [1], in contrast in this study it appears to be the dominate contribution.

There is still the question: Why does this spin-flip mechanism produce the strong alignment of the projectile spin parallel or antiparallel to the beam axis observed in this work? We propose an answer to this question that

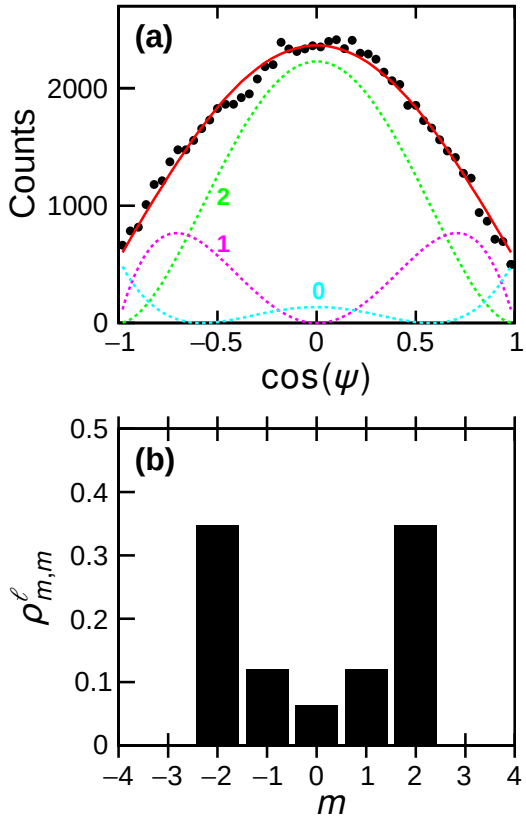

FIG. 10. (Color online) (a) The efficiency-corrected correlation plot for the s^*=3^+ excited state of ^{6}Li projected on the $\cos\psi$ axis. (b) Probability distribution of the projection m of the decay orbital angular momentum. In (a), the solid curve show a fit with the individual m components indicated by the dashed curves.

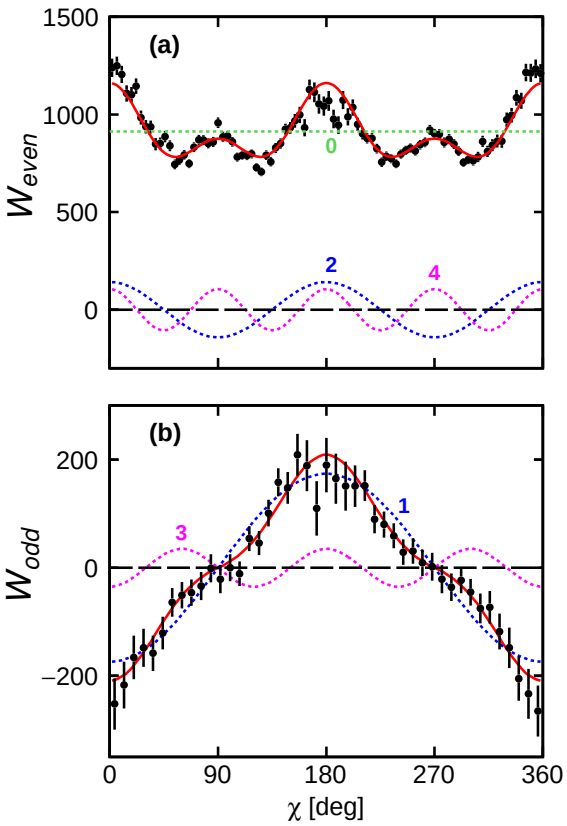

FIG. 11. (Color online) As in Fig. 5, but for the s^*=3^+ excited state of ^{6}Li.

rest on the peculiar structure of the ^{9}Be target nucleus. This nucleus is loosely bound (breakup threshold of only 1.5 MeV) with a very large deformation [37] and strong α-particle structure. It is often modeled as two separated α particles with the valence neutron in a molecular orbit. The ground state corresponds to a spin projection on the symmetry axis of K=3/2 with the valance neutron in the $\pi_{3/2^-}$ orbital, with a degeneracy of two [38].

For the relatively higher-energy reactions studied in this work, one may consider the orientation of the ^{9}Be deformation to remain fixed during the collision. Therefore in flipping the target's spin one is just moving the valence neutron to the other unoccupied member of the $\pi_{3/2^-}$ orbital with opposite angular-momentum projection. This change in spin projection must be facilitated by the interactions of the projectile with the valence neutron, but to prevent this fragile nucleus from breaking up (and keeping it in its ground state), interactions of the projectile with the α-α core should be minimized. This requirement may select certain orientations of the ^{9}Be symmetry axis and thus lead to the strong alignment of the spin of the excited projectiles observed in this work. While the wavefunctions for π orbitals have a node along the symmetry axis, they extend significantly out from this axis. If the symmetry axis is aligned parallel or antiparallel to the beam axis, then such an orientation may allow for projectiles in peripheral trajectories to flip the target nucleus spin without breaking it up. See Fig. 12 for a simplistic depiction of this. Other alignments would lead to a greater probability of the target nucleus breaking up.

VI. CONCLUSION

The sequential breakup of ^{7}Be and ^{6}Li projectiles following inelastic interactions with a ^{9}Be target have been studied. For events where the target nucleus remained in its ground state, we have observed strong alignment of the spin axis for the J^π=$7/2^-$, second excited state of ^{7}Be determined from the angular correlations of the t-α decay products. Similar alignment was also determined for the J^π=3^+, first excited state of ^{6}Li in d-α decay.

The measured angular correlations of the decay products showed strong modulations due to interference between different angular-momentum projections. In addition, both projectiles decay predominantly in the transverse direction corresponding to spin alignments which

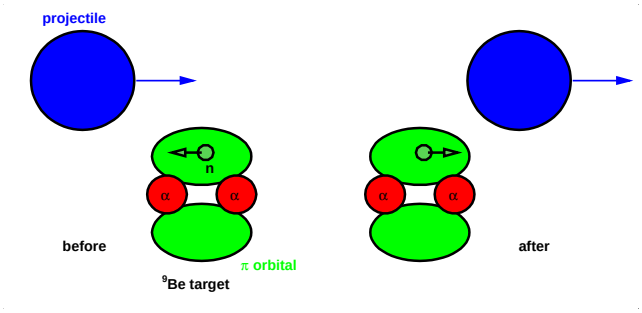

FIG. 12. (Color online) Schematic illustrating the suggested orientation of the target nucleus for the inelastic interactions considered in this work. The ground-state of ^{9}Be target nucleus is depicted as two alpha particles plus a valence neutron in a π molecular orbit. The total angular momentum of the valence neutron is flipped due to interactions with the projectile.

are largely parallel or antiparallel to the beam axis and both excited states have alignments of ∼50%.

The angular correlations were found to have only a small dependence on the projectile scattering angle suggesting that the events are mainly associated with collisions where the orbital angular momentum between the projectile and target does not change. This is further confirmed by the angular distribution of the excited projectiles which peak at zero angle. If the orbital angular momentum does not change, then the change in the projectile's spin from its ground-state value, must be accompanied by a change in orientation of the target's spin alignment, i.e. a target spin flip. The alignments observed in this work are quite different to most other alignment studies in direct reactions where the projectile and target are usually chosen to have zero ground-state spin. In these cases, one often observes alignment perpendicular to the beam axis as changes in the projectile spin must be accompanied by changes in the projectile-target orbital angular momentum.

It is speculated that the strong alignment observed in this work is associated with the structure of ^{9}Be which is very deformed and has a strong α-cluster structure where the valence neutron occupies a π molecular orbit. If the target symmetry axis is aligned with the beam direction, the projectile could more easily interact with the valence neutron, causing the spin flip, without exciting the α-α core. This idea can be tested using the same beams but with a zero-spin target where spin flip is not possible.

Appendix A: Monte Carlo Simulations

The measured correlations, angular distributions and energy spectra were corrected for detector acceptance and resolution using Monte Carlo simulations similar to those discussed in Refs. [30, 31]. In these simulations, the reaction was assumed to occur at a random depth in the secondary target. Energy loss and small-angle scattering of the projectile and the decay products in the target material were then calculated from Refs. [39, 40]. Simulated events were kept if both decay fragments were "detected" in a HiRA telescope. The angles and energies of the "detected" fragments where then smeared by the detector resolutions before being analyzed in the same manner as the experimental events. The acceptance of the HiRA array is governed only by the angular location of the telescopes, which were measured very accurately with a Coordinate Measurement Machine (CMM) arm. Otherwise the energies of the t, ^{3}He, and α decay products from the projectile were located well within the low and high-energy thresholds for detection and identification.

The simulations also included the effects of the beam-spot size and the beam divergence at the target. These quantities were not measured, but a range of reasonable values based on past experiments and predictions were used, and the uncertainties associated with these was included to the error bars of the final efficiency-corrected distributions.

The efficiency as a function of θ^*, used for determining the angular distributions of the scattered projectiles in Figs. 2(c) and 8(b), has a small dependence on the $\psi - \chi$ correlations assumed in the simulation of projectile decay. Similarly the efficiency as functions of ψ and χ as shown in Fig. 3(b) has a small dependency on the projectile angular distribution assumed in the simulations. We therefore employed an iterative approach, starting with an initial guess for both the angular distributions and correlations and then progressively adjusting them both to reproduce the measured distributions. Final efficiencies as a function of the various angle were then calculated from the simulated events and used to correct the experimental distributions.

Appendix B: Spin Alignment of Secondary Beams

Given the unexpected nature of the result, it useful to examine other assumptions made in the analysis. We have assumed that the ^{6}Li and ^{7}Be secondary beams are unpolarized with uniform distributions of their magnetic substates. Fragmentation products can show net polarization and alignment depending on the selected angular and momentum regions [11, 12, 14–18]. Information on the magnetic substate distribution of the beam is contained in a density matrix for beam $\rho^{s_p}_{m_{p1},m_{p2}}$. The secondary beams in this work were produced in a fragmentation of the primary ^{16}O beam and zero-degree products were selected by the A1900 separator. As we expect symmetry about the beam axis, the density matrix should be diagonal [34]. As fully stripped ^{7}Be and ^{6}Li fragments were selected, there was no loss of their polarization or alignment due to the hyperfine interaction during the passage to the secondary target, however, some rotation of the alignment axis will occur due to their passage through the dipole magnets between the primary and sec-

ond targets [41].

If there is any net polarization of the beams, then our assumption that $\rho^{\ell}_{m,m} = \rho^{\ell}_{-m,-m}$ for the excited projectile is not valid and the cancellation of the $\sin(m_1 - m_2)\chi$ terms in Eq. (14) will not occur. Therefore we have refitted the $\cos\psi - \chi$ correlation plots including these $\sin(m_1 - m_2)\chi$ terms but found their magnitudes to be consistent with zero at the 2σ level and thus consistent with zero polarization.

Even if there is no polarization, there may be some alignment, i.e, the magnetic substate distribution is not uniform but $\rho^{s_p}_{m_p,m_p} = \rho^{s_p}_{-m_p,-m_p}$. Such effects in projectile fragmentation have been probed via g-factor measurements of isomers with the Time-Dependent Perturbed Anglar Distribution (TDPAD) method [15–18, 41]. In Ref. [18], the spin aligment is described in a simple model as the net contribution from ablated nucleons removed from a localized region on the surface of the projectile. In this model, the alignment [Eq. (28)] changes from positive to negative as one goes from the peak to the wings of the momentum distribution of the fragmentation products. This is consistent with the limited available data [14–16].

The largest positive alignment has observed from high-spin isomers, e.g., A ∼35% for the I=19/2$^-$ isomer in ^{43}Sc [15]. This is not unexpected, as in such cases the ablated nucleons must act in unison in order to achieve high spins. However for lower-spin isomers, significantly smaller alignments are observed, i.e., for isomers of spin $2 \leqslant I \leqslant 9/2$, only alignments of 9% or less have been observed at the peak of the momentum distribution [14, 16, 18]. In addition, for the low spins the ablation of large numbers of nucleons is expected to further attenuate the alignment as the angular momenta removed by individual nucleons do not have to add, but can cancel. For example an alignment of A=8(1)% was measured for the I=4$^+$ ^{32}Al isomer from the fragmentation of a ^{33}Al beam compared to a limit of A <0.8% from the fragmentation of a ^{48}Ca beam.

Our ^{6}Li and ^{7}Be secondary projectiles have smaller spins than any of these isomer studies and involved significant nucleon loss from the primary ^{16}O projectile. As such we do not expect any appreciable alignment, at most just a few percent. Fragments at the peak of the momentum distribution were selected for the ^{7}Be beam in order to maximize its intensity. Therefore any alignment should be positive. On the other hand, the ^{6}Li beam was a "contaminant" and its yield was far from maximized with a momentum cut away from the peak value. Therefore the expected beam alignment should be even smaller or perhaps negative. However both beams produce alignments of A ∼50% for their excited states thus suggesting the initial beam alignment was unimportant.

Even if our beams were strongly aligned for some unknown reason, one still needs to transfer more aligned angular momentum to the projectile to obtain the larger spin values of the excited states. Clearly if this transfer comes from changes in the projectile's orbital angular moment it is not appropriately aligned in contrast to the proposed target spin-flip mechanism. Thus we conclude that the possible presence of some non-uniformity in the projectile's magnetic-substate distribution is likely to be small and irrelevant.

ACKNOWLEDGMENTS

This material is based upon work supported by the U.S. Department of Energy, Office of Science, Office of Nuclear Physics under Award numbers DE-FG02-87ER-40316, DE-FG02-93ER40773, DE-FG52-09NA29467, and DE-SC004972 and the NSF under grant PHY-0852653.

[1] W. Dünnweber, P. D. Bond, C. Chasman, and S. Kubono, Phys. Rev. Lett. **43**, 1642 (1979).
[2] A. H. Wuosmaa, R. W. Zurmühle, P. H. Kutt, S. F. Pate, S. Saini, M. L. Halbert, and D. C. Hensley, Phys. Rev. Lett. **58**, 1312 (1987).
[3] A. H. Wuosmaa, R. W. Zurmühle, P. H. Kutt, S. F. Pate, S. Saini, M. L. Halbert, and D. C. Hensley, Phys. Rev. C **41**, 2666 (1990).
[4] A. H. Wuosmaa, B. B. Back, R. R. Betts, M. Freer, B. G. Glagola, D. J. Henderson, D. J. Hofman, and V. Nanal, Phys. Rev. C **54**, 2463 (1996).
[5] A. H. Wuosmaa, D. J. Hofman, B. B. Back, D. J. Blumenthal, S. Fischer, D. J. Henderson, R. V. F. Janssens, C. J. Lister, V. Nanal, D. Nisius, M. D. Rhein, and P. R. Wilt, Phys. Rev. C **65**, 024609 (2002).
[6] A. Wuosmaa, I. Wiedenhver, J. Caggiano, M. Carpenter, M. Devlin, A. Heinz, R. Janssens, F. Kondev, T. Lauritsen, D. Sarantites, L. Sobotka, and P. Battacharyya, Physics Letters B **571**, 155 (2003).
[7] G. J. Wozniak, R. J. McDonald, A. J. Pacheco, C. C. Hsu, D. J. Morrissey, L. G. Sobotka, L. G. Moretto, S. Shih, C. Schück, R. M. Diamond, H. Kluge, and F. S. Stephens, Phys. Rev. Lett. **45**, 1081 (1980).
[8] L. G. Sobotka, C. C. Hsu, G. J. Wozniak, G. U. Rattazzi, R. J. McDonald, A. J. Pacheco, and L. G. Moretto, Phys. Rev. Lett. **46**, 887 (1981).
[9] L. Sobotka, C. Hsu, G. Wozniak, D. Morrissey, and L. Moretto, Nuclear Physics A **371**, 510 (1981).
[10] D. Morrissey, G. Wozniak, L. Sobotka, R. McDonald, A. Pacheco, and L. Moretto, Nuclear Physics A **442**, 578 (1985).
[11] K. Asahi, M. Ishihara, N. Inabe, T. Ichihara, T. Kubo, M. Adachi, H. Takanashi, M. Kouguchi, M. Fukuda, D. Mikolas, D. Morrissey, D. Beaumel, T. Shimoda, H. Miyatake, and N. Takahashi, Physics Letters B **251**, 488 (1990).
[12] H. Okuno, K. Asahi, H. Sato, H. Ueno, J. Kura, M. Adachi, T. Nakamura, T. Kubo, N. Inabe, A. Yoshida,

T. Ichihara, Y. Kobayashi, Y. Ohkubo, M. Iwamoto, F. Ambe, T. Shimoda, H. Miyatake, N. Takahashi, J. Nakamura, D. Beaumel, D. Morrissey, W.-D. Schmidt-Ott, and M. Ishihara, Physics Letters B **335**, 29 (1994).

[13] L. V. Chulkov, T. Aumann, D. Aleksandrov, L. Axelsson, T. Baumann, M. J. G. Borge, R. Collatz, J. Cub, W. Dostal, B. Eberlein, T. W. Elze, H. Emling, H. Geissel, V. Z. Goldberg, M. Golovkov, A. Grünschloss, M. Hellström, J. Holeczek, R. Holzmann, B. Jonson, A. A. Korsheninnikov, J. V. Kratz, G. Kraus, R. Kulessa, Y. Leifels, A. Leistenschneider, T. Leth, I. Mukha, G. Münzenberg, F. Nickel, T. Nilsson, G. Nyman, B. Petersen, M. Pfützner, A. Richter, K. Riisager, C. Scheidenberger, G. Schrieder, W. Schwab, H. Simon, M. H. Smedberg, M. Steiner, J. Stroth, A. Surowiec, T. Suzuki, and O. Tengblad, Phys. Rev. Lett. **79**, 201 (1997).

[14] K. Asahi, M. Ishihara, T. Ichihara, M. Fukuda, T. Kubo, Y. Gono, A. C. Mueller, R. Anne, D. Bazin, D. Guillemaud-Mueller, R. Bimbot, W. D. Schmidt-Ott, and J. Kasagi, Phys. Rev. C **43**, 456 (1991).

[15] W.-D. Schmidt-Ott, K. Asahi, Y. Fujita, H. Geissel, K.-D. Gross, T. Hild, H. Irnich, M. Ishihara, K. Krumbholz, V. Kunze, A. Magel, F. Meissner, K. Muto, H. Okuno, M. Pfützner, C. Scheidenberger, K. Suzuki, M. Weber, and C. Wennemann, Z. Phys. A **350**, 215 (1994).

[16] I. Matea, G. Georgiev, J. M. Daugas, M. Hass, G. Neyens, R. Astabatyan, L. T. Baby, D. L. Balabanski, G. Bélier, D. Borremans, G. Goldring, H. Goutte, P. Himpe, M. Lewitowicz, S. Lukyanov, V. Méot, F. de Oliveira Santos, Y. E. Penionzhkevich, O. Roig, and M. Sawicka, Phys. Rev. Lett. **93**, 142503 (2004).

[17] M. Kmiecik, A. Maj, J. Gerl, G. Neyens, L. Atanasova, D. Balabanski, F. Becker, P. Bednarczyk, G. Benzoni, N. Blasi, A. Bracco, S. Brambilla, L. Caceres, F. Camera, M. Ciemaa, F. Crespi, S. Chamoli, S. Chmel, J. Daugas, P. Detistov, P. Doornenbal, G. Georgiev, K. Gladnishki, M. Górska, H. Grawe, J. Gręboszc, M. Hass, R. Hoischen, G. Ilie, M. Ionescu-Bujor, J. Jolie, I. Kojuharov, A. Krasznahorkay, R. Kulessa, M. Lach, S. Lakshmi, S. Leoni, G. Lo Bianco, R. Lozeva, K. Maier, S. Mallion, K. Mazurek, W. Męczński, B. Million, D. Montanari, S. Myalski, C. Petrache, M. Pfützner, S. Pietri, Z. Podolyák, W. Prokopowicz, D. Rudolph, N. Saito, T. Saito, A. Saltarelli, G. Simpson, J. Styczeń, N. Vermeulen, E. Werner-Malento, O. Wieland, H. Wollersheim, and Zięblński, Eur. Phys. J. A **45**, 153 (2010).

[18] Y. Ichikawa, H. Ueno, Y. Ishii, T. Furukawa, A. Yoshimi, D. Kameda, H. Watanabe, N. Aoi, K. Asahi, D. L. Balabanski, R. Chevrier, J.-M. Daugas, N. Fukuda, G. Georgiev, H. Hayashi, H. Iijima, N. Inabe, T. Inoue, M. Ishihara, T. Kubo, T. Nanao, T. Ohnishi, K. Suzuki, M. Tsuchiya, H. Takeda, and M. M. Rajabali, Nat. Phys. **8**, 918 (2012).

[19] K. Skarsvåg, Phys. Rev. C **22**, 638 (1980).

[20] Y. N. Kopach, P. Singer, M. Mutterer, M. Klemens, A. Hotzel, D. Schwalm, P. Thirolf, M. Hesse, and F. Gönnenwein, Phys. Rev. Lett. **82**, 303 (1999).

[21] S. G. Steadman, T. A. Belote, R. Goldstein, L. Grodzins, D. Cline, M. J. A. de Voigt, and F. Videbæk, Phys. Rev. Lett. **33**, 499 (1974).

[22] F. Pougheon, P. Roussel, M. Bernas, F. Diaf, B. Fabbro, F. Naulin, E. Plagnol, and G. Rotbard, Nuclear Physics A **325**, 481 (1979).

[23] H. G. Bohlen, W. Bohne, B. Gebauer, W. von Oertzen, M. Goldschmidt, H. Hafner, L. Pflug, and K. Wannebo, Phys. Rev. Lett. **37**, 195 (1976).

[24] G. Ingold, H. G. Bohlen, M. Clover, H. Lettau, H. Ossenbrink, and W. von Oertzen, Z. Phys. A **305**, 135 (1982).

[25] W. Rae and R. Bhowmik, Nuclear Physics A **420**, 320 (1984).

[26] E. Costanzo, M. Lattuada, S. Romano, D. Vinciguerra, N. Cindro, M. Zadro, M. Freer, B. R. Fulton, and W. D. M. Rae, Phys. Rev. C **44**, 111 (1991).

[27] S. P. G. Chappell and W. D. M. Rae, Phys. Rev. C **53**, 2879 (1996).

[28] M. Freer, Nuclear Instruments and Methods in Physics Research Section A: Accelerators, Spectrometers, Detectors and Associated Equipment **383**, 463 (1996).

[29] K. J. Honkanen, F. A. Dilmanian, D. G. Sarantites, and S. P. Sorensen, Nucl. Instr. and Meth. **262A**, 366 (1987).

[30] R. J. Charity, J. M. Elson, J. Manfredi, R. Shane, L. G. Sobotka, Z. Chajecki, D. Coupland, H. Iwasaki, M. Kilburn, J. Lee, W. G. Lynch, A. Sanetullaev, M. B. Tsang, J. Winkelbauer, M. Youngs, S. T. Marley, D. V. Shetty, A. H. Wuosmaa, T. K. Ghosh, and M. E. Howard, Phys. Rev. C **82**, 041304 (2010).

[31] R. J. Charity, J. M. Elson, J. Manfredi, R. Shane, L. G. Sobotka, B. A. Brown, Z. Chajecki, D. Coupland, H. Iwasaki, M. Kilburn, J. Lee, W. G. Lynch, A. Sanetullaev, M. B. Tsang, J. Winkelbauer, M. Youngs, S. T. Marley, D. V. Shetty, A. H. Wuosmaa, T. K. Ghosh, and M. E. Howard, Phys. Rev. C **84**, 014320 (2011).

[32] M. S. Wallace, M. A. Famiano, M.-J. V. Goethem, A. Rogers, W. G. Lynch, J. Clifford, J. Lee, S. Labostov, M. Mocko, L. Morris, A. Moroni, B. E. Nett, D. J. Oostdyk, R. Krishnasamy, M. B. Tsang, R. D. de Souza, S. Hudan, L. G. Sobotka, R. J. Charity, J. Elson, and G. L. Engel, Nucl. Instrum. Methods A (2007).

[33] A. Strazzeri, *On the general form of the particle angular correlation following the sequential decay of the heavy reaction product in one-level excitation hypothesis.-(I). Double Angular Correlation*, Report CRN-PN-78-15 (Center de Recherches Nucléaires, Strasbourg, France, 1978) also available on the internet from the International Nuclear Information System, Ref. number 10481601.

[34] G. R. Satchler, *Direct Nuclear Reactions* (Oxford University Press, Oxford, 1983).

[35] G. R. Satchler, Nucl. Phys. **55**, 1 (1964).

[36] N. Austern, *Direct Nuclear Reaction Theories* (Wiley, New York, 1970).

[37] Evaluated Nuclear Structure Data File (ENSDF), http://www.nndc.bnl.gov/ensdf/.

[38] W. von Oertzen, Z. Phys. A **354**, 43 (1996).

[39] J. F. Ziegler, J. P. Biersack, and U. Littmark, *The Stopping and Range of Ions in Solids* (Pergamon Press, New York, 1985) the code SRIM can be found at www.srim.org.

[40] R. Anne, J. Herault, R. Bimbot, H. Gauvin, C. Bastin, and F. Hubert, Nucl. Instrum. Methods B **34**, 295 (1988).

[41] G. Georgiev, G. Neyens, M. Hass, D. L. Balababski, C. Bingham, C. Borcea, N. Coulier, R. C. J. M. Daugas, G. De France, F. de Oliveira Santos, M. Górska, H. Grawe, R. Grzywacz, M. Lewitowicz, H. Mach, R. D. Page, M. Pfützner, Y. E. Penionzhkevich, Z. Podolyák, P. H. Regan, K. Rykaczewski, M. Sawicka, N. A. Smirnova, Y. G. Sobolev, M. Stanoiu, S. Teughels, and K. Vyvey, J. Phys. G **28**, 2993 (2002).